Journal of Materials Science: Materials in Electronics (2018) 29:19086–19098
https://doi.org/10.1007/s10854-018-0035-8

Significant improvement in morphological, dielectric, ferroelectric and piezoelectric characteristics of $Ba_{0.9}Sr_{0.1}Ti_{0.9}Zr_{0.1}O_3$–$BaNb_2O_6$ nanocomposites

Aditya Jain[1] · Amrish K. Panwar[1] · A. K. Jha[2]

Received: 30 March 2018 / Accepted: 7 September 2018 / Published online: 14 September 2018

Abstract
Multifunctional composite with material composition $(1-x)Ba_{0.9}Sr_{0.1}Ti_{0.9}Zr_{0.1}O_3$–$xBaNb_2O_6$ ($x=0.0$, 0.05, 0.1, 0.2 and 0.3) has been successfully synthesized using mechano-chemical activation process. The co-existence of perovskite tetragonal phase of BSTZ and niobate orthorhombic phase of BNO was detected by X-ray diffraction measurement and confirmed by Rietveld analysis. All the BSTZ–BNO composites show a polygonal grain type morphology with clearly visible grain boundaries. BSTZ–BNO composites possessed a thermally stable dielectric constant within a broad range of temperature. The obtained results show a strong influence of BNO addition on the microstructural, dielectric, ferroelectric, piezoelectric and breakdown strength of bare BSTZ ceramic. For $x=0.10$, the composite exhibit optimum properties with high dielectric constant $\varepsilon_m=5842$, large remnant polarization $P_r=9.25$ μC/cm^2, improved piezoelectric constant $d_{33}=296$ pC/N and high breakdown strength $E_{bd}=304$ kV/cm. The high dielectric constant accompanied by very low dielectric loss and large piezoelectric constant make BSTZ–BNO a suitable material for ceramic capacitors and electromechanical device applications.

1 Introduction

Miniaturization of solid state electronic devices has been accomplished by multifunctionality and downscaling. Multifunctional ceramic composites have drawn much attention in recent owing to their promising applications in novel technological devices. Characteristically, they possess more than one order parameter which can be coupled to one another. $BaTiO_3$ based composite materials and investigation of their properties have attracted much recognition with advances of novel procedures for the development of perovskite and phosphor materials, expanding their usage in other areas, for example, light emitting devices, ceramic capacitors, microwave devices, field emission devices, etc. [1]. On the other hand, micro and nano-electronics research in the larger portion is driven by the need for smaller component devices exhibiting better performance. For capacitive components, those are considered as an integral part of many memory devices for example, read-only memory (ROM), random access memory (RAM) and USB flash drives, the dielectric constant of the materials restricts the degree of miniaturization—a limit that has been rigorously attempted to overcome in the last decade. Till now, improvement in dielectric constant value has been attained by using mainly barium zirconium titanate, barium strontium titanate, etc. [2, 3].

Among lead-free ferroelectric materials, (Ba,Sr)(Zr,Ti)O_3 have been paid much consideration for their possible application in dielectric tunable devices and dynamic random access memories. It has been observed that the diffuse phase transition in BSTZ is advantageous in attaining better piezoelectric properties and high electrocaloric constant [4]. In these materials, the ferroelectric and optical characteristics along with degree of coupling are mainly reliant on the microstructure, including the domain pattern as well as grain shape [5]. In the present study, $Ba_{0.9}Sr_{0.1}Ti_{0.9}Zr_{0.1}O_3$ (BSTZ) has been taken as the host matrix. BSTZ exhibit a perovskite structure (ABO_3), where barium and strontium occupy the A-site and titanium and zirconium occupy the B-site of the lattice. In BSTZ, various characteristics such as dielectric

Electronic supplementary material The online version of this article (https://doi.org/10.1007/s10854-018-0035-8) contains supplementary material, which is available to authorized users.

✉ Amrish K. Panwar
panwaramar@gmail.com

[1] Lithium Ion Battery Technology Lab, Delhi Technological University, New Delhi 110042, India

[2] Department of Applied Science, A.I.A.C.T.R., Geeta Colony, New Delhi 110031, India

constant, transition temperature, electrical resistance, etc. can be efficiently manipulated by combining it with individual compounds or dopants.

Niobate group materials have attracted much consideration by researchers owing to their promising piezoelectric, pyroelectric, electro-optic and nonlinear properties combined with their industrial as well as scientific applications in the area of photonics, microwave dielectric materials, holographic storage devices and frequency doublers [6]. Amongst all the intrinsic alkaline earth meta-niobate compounds such as, $CaNb_2O_6$, $SrNb_2O_6$ and $BaNb_2O_6$, the charge generation in $BaNb_2O_6$ was found to be higher which is attributed to smaller energy band gap as compared to other meta-niobates materials [7, 8]. Microwave dielectric properties and photocatalytic activities of barium niobates have been copiously explored in recent time [2, 9, 10]. Till now, numerous groups of materials have been studied to improve the ferroelectric ordering and electro-optical properties, but still, particular attention has been paid to lead-free composites due to their better electro-optical coupling and environmental friendliness [11, 12]. However, a detailed literature survey reveals that the investigation of ferroelectric and piezoelectric properties along with electrical breakdown strength of $Ba_{0.9}Sr_{0.1}Ti_{0.9}$ $Zr_{0.1}O_3$–$BaNb_2O_6$ (BSTZ–BNO) has not been reported so far.

It is a well-known fact that conventional high energy ball milling technique can be used for synthesizing crystalline micro and nano-composites. This technique has many benefits, for example, applicability to any class of materials, production simplicity and relatively inexpensive synthesis [13–15]. Mechanochemical activation technique has another benefit that it can initiate solid-state reactions at comparatively lesser temperature than those required in conventional techniques of material synthesis. In the present work, $(1-x)$ $Ba_{0.9}Sr_{0.1}Ti_{0.9}Zr_{0.1}O_3$–$(x)BaNb_2O_6$ has been prepared via conventional ball milling technique and their morphological, electrical and optical characteristics have been explored rigorously. The aim of the current investigation is to examine the orientation and mixed phase properties of BSTZ–BNO composites.

2 Experimental

Particulate composite with $Ba_{0.9}Sr_{0.1}Ti_{0.9}Zr_{0.1}O_3$ (BSTZ) as a host material and $BaNb_2O_6$ (BNO) as another part of the composite material were prepared by conventional ball milling technique. $Ba_{0.9}Sr_{0.1}Ti_{0.9}Zr_{0.1}O_3$ was synthesized by taking high-purity Sigma-Aldrich make analytical reagent grade chemicals barium carbonate (99.99%), strontium carbonate (99.9%), titanium dioxide (99.8%) and zirconium dioxide (99.0%) as the raw materials. All raw chemicals were mixed in the required ratio, which is followed by ball milling in an air environment at 475 rpm for 24 h. Ball milling of the samples was carried out using *Retsch make* planetary ball mill. A jar made of ZrO_2 having 50 ml capacity, 45 mm diameter along with 125 Zirconia balls of 5 mm diameter have been used as milling environment. Initially, the as-prepared BSTZ solid solution was calcined at 1025 °C for 5 h at a slow heating rate of 3 °C/min. The calcination was followed by sintering for 4 h at an optimized temperature of 1260 °C.

Extremely pure analytical reagent grade Barium carbonate (99.99%) and Niobium pentoxide (99.99%) in stoichiometric proportion were milled alongside Toluol to synthesize the $BaNb_2O_6$ solid solution for 24 h in the same environment as used for preparing BSTZ. The milled powder was calcinated at 625 °C for 1 h which is followed by high-temperature sintering at 1200 °C for 5 h. Subsequently, these composite solid solutions $(1-x)$ $Ba_{0.9}Sr_{0.1}Ti_{0.9}Zr_{0.1}O_3$–$(x)$ $BaNb_2O_6$ (where $x=0$, 5, 10, 20 and 30 wt%) were collected by thoroughly blending the constituent phases BSTZ and BNO in required proportion inside the ball milling for effective 8 h. The as obtained sintered composite solid solutions were finally blended with 3 wt% of water-soluble synthetic polymer 'polyvinyl alcohol' followed by pressing them into thin cylindrical pellets of 8 mm diameter and nearly thickness of 0.8 mm by applying a force of 75 kN using a pelletizer. The pellets were then heated in air environment at 600 °C. Henceforward, these composites are termed as BBN0, BBN5, BBN10, BBN20 and BBN30 having the weight ratio of $x=0$, 0.05, 0.10, 0.20 and 0.30, respectively.

Bruker D8 Advance X-ray diffractometer has been used to determine the crystallographic structure and phase of BBNx composites. Rietveld refinement of BSTZ–BNO composites was carried out using a computer program package *X'Pert Highscore Plus*. The surface morphology, microstructural features and grain size were examined using *Hitachi S-3700N* scanning electron microscope. Grain size distribution analysis of SEM images has been performed using *ImageJ* software. TEM, HRTEM and SAED study of the optimized sample has been performed using TEM (JEOL 3010) operating at 270 kV. For further electrical measurements, electrodes were designed by coating silver paste on both faces of pellet samples, which was followed by curing the pellets at 150 °C for 10 min. The obtained pellets were then used to measure dielectric characteristics by using an *Agilent 4284A* LCR meter operating at wide range of frequencies over a broad temperature range of 25–200 °C. The electric field versus polarization hysteresis characteristics of all the composite specimens were measured using E–P loop analyzer (*M/s Marine India, New Delhi*). Piezoelectric properties measurement of the samples was carried out using *PIEZOTEST* system UK. Measurement of dielectric breakdown strength (E_{bd}) were carried out on a sample coated with silver paste. This electroded sample is dipped in a bath

filled with silicon oil and placed on a baseplate of high conductivity copper.

3 Result and discussion

3.1 X-ray diffraction (XRD)

To comprehend the structural and phase modification with the addition of $BaNb_2O_6$ in $Ba_{0.9}Sr_{0.1}Ti_{0.9}Zr_{0.1}O_3$, Rietveld technique has been used for structural refinement. Figure 1a demonstrate the comparative XRD patterns of $(1-x)Ba_{0.9}Sr_{0.1}Ti_{0.9}Zr_{0.1}O_3$–$xBaNb_2O_6$ ($x=0$, 0.05, 0.1, 0.2 and 0.3). The intense and sharp XRD peaks indicate the crystalline nature of the bare and composite samples. The dotted rectangular boxes indicate that as BNO content increases, some extra peaks begin to appear in the XRD pattern. Figure 1b–f depicts the Rietveld-refined XRD patterns of $(1-x)$BSTZ–(x)BNO. Barium titanate (JCPDS database no. 000-005-0626) and barium niobate (JCPDS database no. 001-077-0589) were considered as the reference diffraction patterns. A clear and well-identifiable tetragonal phase with P4*mm* space group is detected for BBN0, although, as the BNO concentration is increased, the diffraction peaks of barium niobate start appearing. The BSTZ–BNO composites synthesized using the mechano-chemical activation

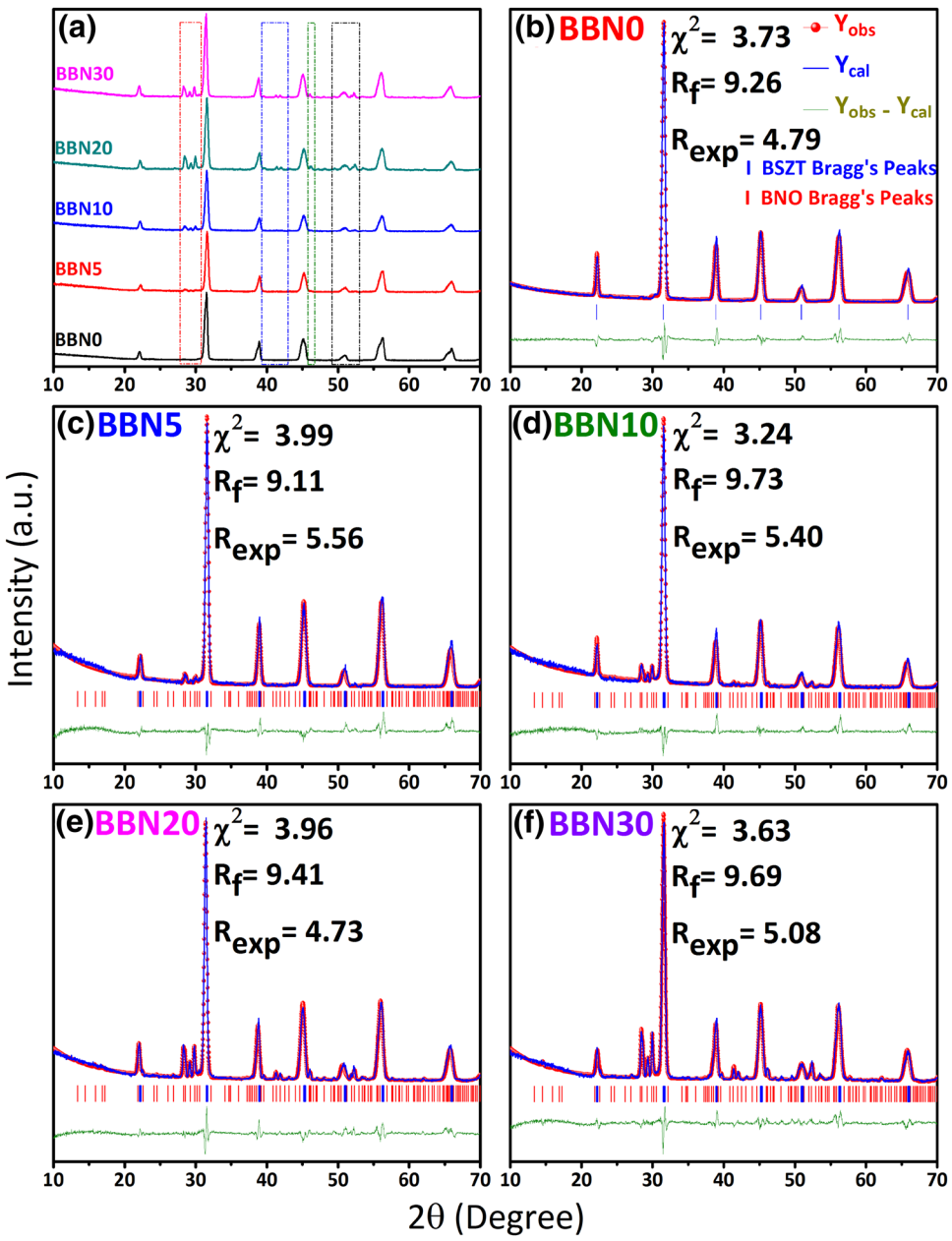

Fig. 1 Comparative and Rietveld refined XRD spectra of as-synthesized $(1-x)$BSTZ–xBNO composite ceramics: **a** combined XRD spectra of all the five samples **b** $x=0.0$, **c** $x=0.05$, **d** $x=0.10$, **e** $x=0.20$ and **f** $x=0.30$

technique exhibited a mixed tetragonal-orthorhombic structure and did not show any significant observable impurity. The calculated and observed *d* spacing values of all the diffraction peaks in bare and composite samples specify that there is no change in the parent crystal structure (tetragonal) as *x* is increased from 0.05 to 0.3. However, there is a slight change in tetragonality of the samples, which is attributed to change in lattice parameters *'a'* and *'c'* changes with an increase in BNO content.

Further, the results approve the successful synthesis of the di-phasic composite materials. Further, this also suggests that both (BSTZ and BNO) the parent phases have retained their basic identity in the composite materials and no unwanted reaction took place between the ferroelectric BSTZ and phosphor BNO phases during the final annealing of the materials. The host ferroelectric BSTZ phase of the composite exhibit a P4*mm* space group and crystallizes in a tetragonal structure whereas, BNO has an orthorhombic structure with $C222_1$ space group. It was observed that the intensity of diffraction peaks of the orthorhombic phase increases with increase in BNO content. The detailed structural parameters achieved after the Rietveld refinement analysis are shown in Table 1. By observing at the XRD pattern of composites, it can be concluded that at higher BNO content samples limited reaction took place amid the ferroelectric-phosphor phases of BSTZ and BNO, respectively. Figure 2a, b demonstrate the as obtained crystal structure of both the compounds i.e. BSTZ and BNO. The crystal structures were obtained with the help of VESTA software from the refined atomic positions found after the Rietveld analysis of BBN10 composite. The blue and light green colored stripes at Barium and Titanium site show the occupancy of strontium and zirconium ions, respectively. Further, the obtained atomic positions also confirm that in BBN10 sample, the BSTZ exists in tetragonal phase and BNO is present in orthorhombic phase.

3.2 Microstructural studies

SEM micrographs of five synthesized specimens are depicted in the Fig. 3a–e. All the samples exhibit dense grain structure with clearly distinguished grain boundaries. The grain size and homogeneity of these composites were significantly affected by BNO addition. However, the surface morphology was found to be relatively identical. BBN10 sample shows fairly homogeneously distributed grains compared to BBN20 and BBN30, both of which reveals rather more inhomogeneous grain distribution. The average grain size of these samples was found to be approximately 1.51, 1.44, 1.61, 1.76 and 1.81 μm for BBN0, BBN5, BBN10, BBN20

Table 1 Rietveld refined XRD parameters for bare BSTZ and BSTZ–BNO composite samples

Sample	Space group	Crystal structure	Lattice parameters (Å)	Cell volume (Å^3)	χ^2	R_{exp}	R_f	R_{Bragg}
BBN0	*P4mm*	Tetragonal	a = 4.0125 c = 4.0257	64.8154	3.73	4.79	9.26	3.03
BBN5								
BSTZ phase	*P4mm*	Tetragonal	a = 4.0051 c = 4.0291	64.6306	3.99	5.56	9.11	6.16
BNO phase	$C222_1$	Orthorhombic	a = 7.8712 b = 12.201 c = 10.268	987.727				4.16
BBN10								
BSTZ phase	*P4mm*	Tetragonal	a = 4.0047 c = 4.0278	64.5963	3.24	5.40	9.73	5.79
BNO phase	$C222_1$	Orthorhombic	a = 7.8615 b = 12.210 c = 10.277	986.600				3.83
BBN20								
BSTZ phase	*P4mm*	Tetragonal	a = 4.0038 c = 4.0251	64.5226	3.96	4.73	9.41	3.09
BNO phase	$C222_1$	Orthorhombic	a = 7.8608 b = 12.193 c = 10.272	984.670				3.92
BBN30								
BSTZ phase	*P4mm*	Tetragonal	a = 3.9966 c = 4.0168	64.1611	3.63	5.08	9.63	2.65
BNO phase	$C222_1$	Orthorhombic	a = 7.8400 b = 12.159 c = 10.248	977.627				4.01

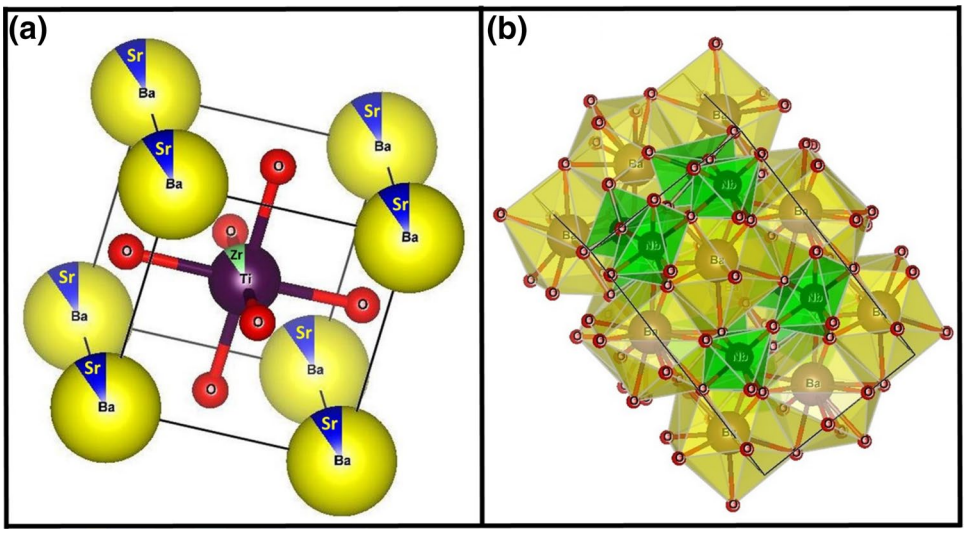

Fig. 2 Crystal structure of **a** BSTZ and **b** BNO; drawn from the atomic positions obtained after the Rietveld analysis of BBN10 sample

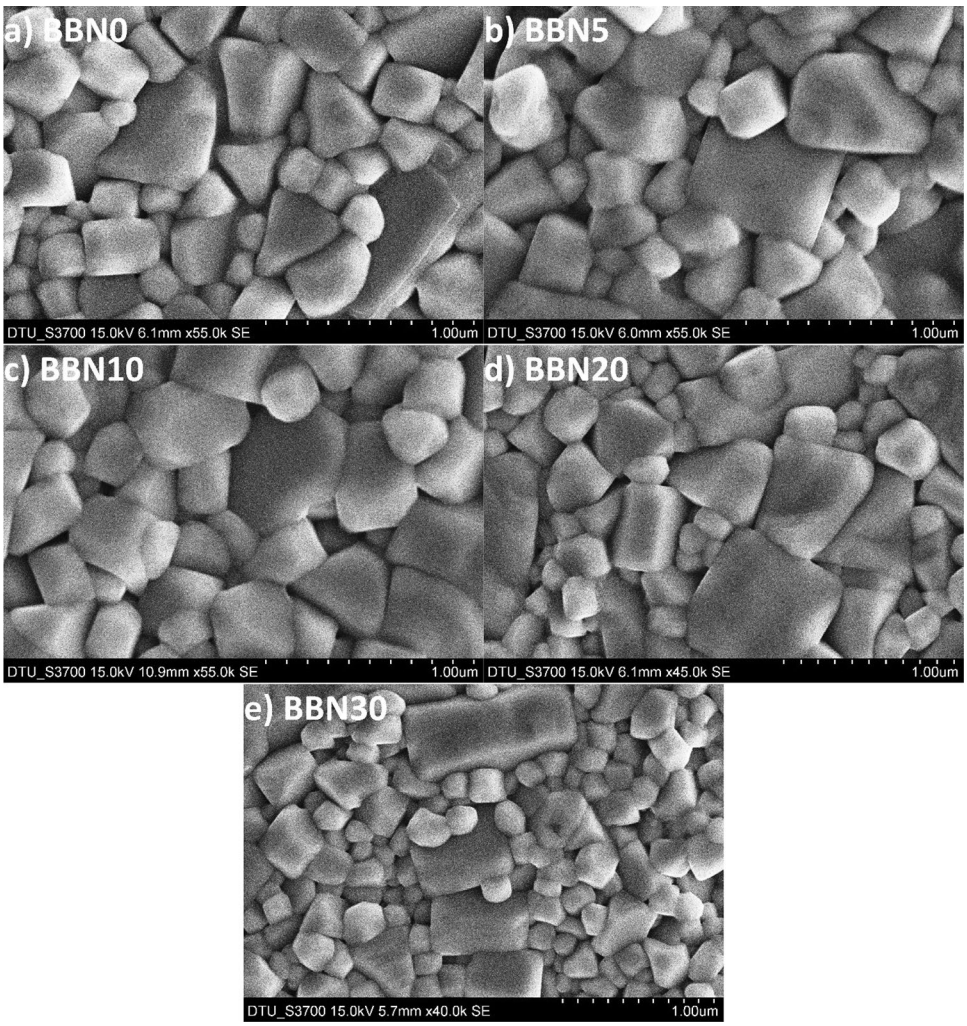

Fig. 3 SEM micrograph of high temperature sintered pellets of $(1-x)$BSTZ–xBNO composites: **a** $x=0.0$, **b** $x=0.05$, **c** $x=0.10$, **d** $x=0.20$ and **e** $x=0.30$

Table 2 Room temperature saturation polarization (P_s), remnant polarization ($2P_r$), coercive field ($2E_c$), breakdown strength (E_{bd}) and piezoelectric constant (d_{33}) for bare BSTZ and BSTZ–BNO composite samples

Sample	Relative density	$2P_s$ (μC/cm^2)	$2P_r$ (μC/cm^2)	$2E_c$ (kV/cm)	E_{bd} (kV/cm)	d_{33} (pC/N)
BBN0	5.697	17.0	5.5	4.8	235	269
BBN5	5.701	33.8	15.4	15.9	267	302
BBN10	5.719	36.7	18.5	18.8	304	296
BBN20	5.671	24.1	13.4	13.8	249	241
BBN30	5.673	20.2	8.62	9.1	223	176

and BBN30, respectively. Further, to clearly understand the grain growth and porosity inside the material, authors have carried out the density measurement of all the five samples and shown in Table 2. The piezoelectric properties of polycrystalline materials are affected by both intrinsic and extrinsic parameters [16, 17]. The grain size as extrinsic parameter strongly affect the piezoelectric properties of any material. In earlier reports, it has been reported that coarse-grained ceramics show improved piezoelectric response compared to finely-grained ceramics [18]. Moreover, the coarse grain ceramics facilitate better polarization and enhanced domain mobility, resulting in a higher degree of polarization in the material and hence superior electrical properties [19, 20]. Furthermore, it is eminent that the grain size as well as the morphology of the ceramics heavily rely on its calcination and sintering temperature along with the soaking time span at the peak temperature [21, 22]. These two aspects also change the microstructure of the final sintered sample and henceforth, they affect the electrical characteristics of the ceramic materials. In higher BNO content composites, the occurrence of two types of grains having a significant difference in grain size may be attributed to the fact that the particles of one phase may have a higher likelihood of growing as compared other at higher sintering temperature and consequently larger grains grows at the cost of smaller grains. Furthermore, in case of composites, it is rather strenuous to produce a homogeneous morphology along with uniform grain size owing to the significant difference in the optimum heating environments and the thermal expansion constant of two different compounds.

TEM and HRTEM imaging of BBN10 has been carried out since it demonstrates overall superior dielectric, ferroelectric and piezoelectric characteristics among all the synthesized specimens. The TEM technique offers valuable insight in identifying the particle morphology and intergrowth of a material. The average particle size of BBN10 solid solution obtained using TEM study is shown in Fig. 4a were found to be ~ 160 nm. These parallelly aligned lattice fringes in the HRTEM image of BBN10 shows that the sample is perfectly crystalline. The HRTEM images of BBN10 particle depicted in Fig. 4b, c demonstrate the lattice fringes corresponding to various planes having an inter-fringe distance of 1.35 Å, 1.69 Å and 1.57 Å, respectively. In Fig. 4c, a twinned region is marked with a triangle, that may be identified as an area where $Ba_{0.9}Sr_{0.1}Ti_{0.9}Zr_{0.1}O_3$ and $BaNb_2O_6$ particles have submerged into one another and subsequently leading to twinning of the lattice fringes. The Prallelly aligned lattice fringes in the HRTEM image of BBN10 having an inter-fringe distance of 1.35 Å and 1.69 Å can be allocated to BSTZ phase with corresponding (212) and (112) planes having conventional d spacing value of 1.34 Å and 1.66 Å, respectively. Also, the lattice fringes located inside the twinned interface with 1.57 Å inter-fringe distance can be allocated to BNO phase with analogous (442) plane with 1.575 Å as the conventional d spacing. Figure 4d depicts the selected area electron diffraction (SAED) pattern which is in good agreement with HRTEM results and approves the crystalline nature of BBN10 specimen. The bright and dark spots in SAED pattern can be allocated to various planes in the tetragonal and orthorhombic crystal. The SAED pattern was measured for the twinned region of the HRTEM image that demonstrates two sets of bright and dark spots confirming the diffusion of BSTZ and BNO compounds for observed area. Furthermore, both of the HRTEM image as well as SAED patterns investigated for the specimen having optimum properties i.e. BBN10, shows no noteworthy structural defects upon HRTEM investigation.

3.3 Dielectric studies

The temperature dependency of dielectric characteristics of BSTZ–BNO composite materials have been investigated and are shown in Fig. 5a–e. The inset of the dielectric curve shows the magnified view of variation in dielectric constant with temperature. The dielectric properties were studied at eight different frequencies. BNO addition in BSTZ lattice has resulted in a significant change in phase transition characteristics as compared to BNO free BSTZ sample. At lower frequency, BNO substituted samples show a sharp transition compared to the bare sample, however, at high frequency, the phase transition becomes progressively diffused (flattened and broad) type. The occurrence of a single broad peak in BBN0 and comparatively narrower peak in composite samples signifies the transition of ferroelectric to paraelectric phase or tetragonal to cubic phase. Further, the dielectric constant (ε_m) at phase transition temperature decreases with even a small rise in frequency and is observed to be minimum at 1 MHz. It is observed that permittivity maxima

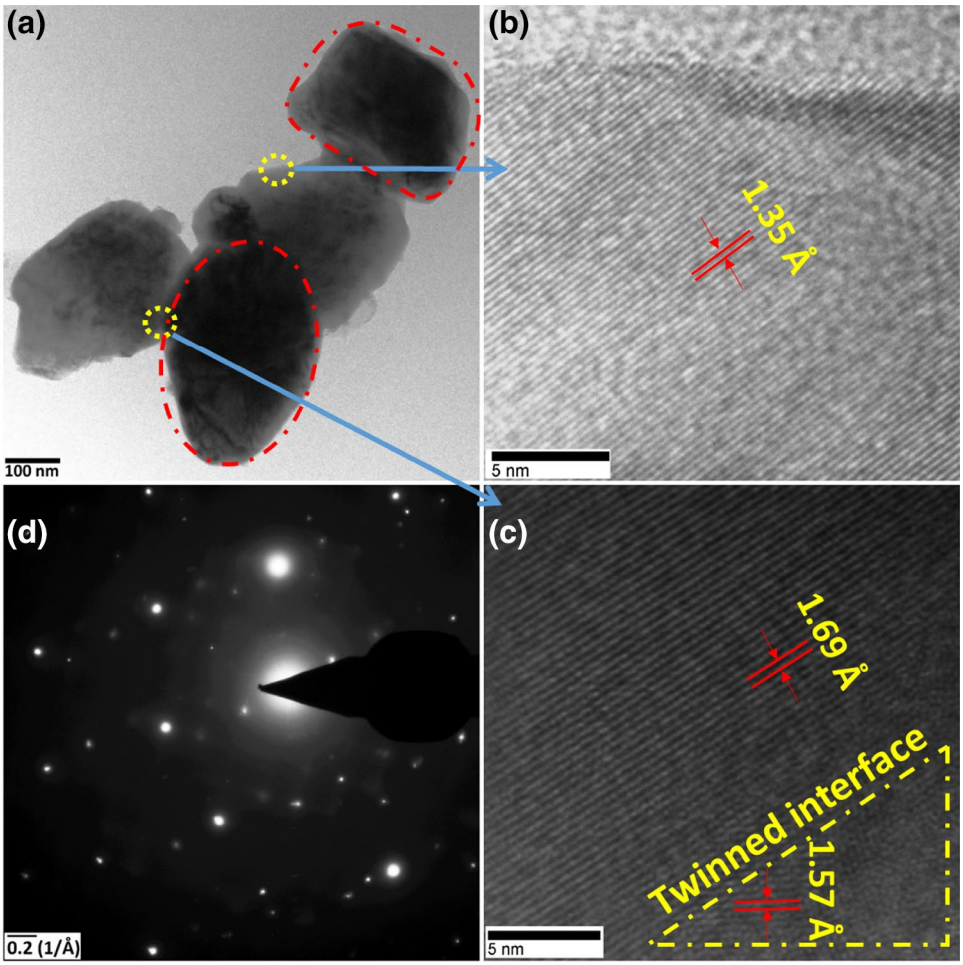

Fig. 4 TEM/HRTEM micrographs of BBN10: **a** TEM, **b, c** HRTEM, **d** SAED pattern

of BBN5 and BBN10 have been enhanced compared with that of BNO free BSTZ sample. The dielectric constant of the samples shows a gradual rise with an increase in BNO concentration becomes maximum for BBN10 composite and decreases on further increasing the BNO concentration. The dielectric constant at phase transition temperature for the samples BBN0, BBN5, BBN10, BBN20 and BBN30 at 20 Hz was found to be ~4361, 5105, 5842, 3570 and 2547, respectively. The high dielectric constant of BBN10 sample may be due to optimum grain size, grain homogeneity as well as higher density of the material among all the prepared samples. Larger grain size corresponds to less number of insulating grain boundaries layers. This decrease in number of grain boundaries leads to lesser trapping of space charge and thus lesser domain wall pinning resulting in overall high dielectric constant [23, 24]. One more possibility for the reduction in dielectric constant at higher BNO concentration might be due to inhibition of Nb^{5+} at Ti^{4+}/Zr^{4+} site of ABO_3 perovskite unit cell, resulting in weakening of bonding force between the oxygen atom and B-site ion. A clear ferroelectric to paraelectric phase transition peak can be seen for all the five samples, which clearly indicate that even at higher BNO concentration dielectric properties of the composites are still governed by BSTZ phase.

At high frequency, the dielectric properties of BSTZ–BNO composites become frequency independent. Moreover, considering only the high-frequency characteristics, the phase transition curve appears to be more diffusive compared to BNO free BSTZ sample. This indicates that the addition of BNO results in a gradual transformation from typical ferroelectric to relaxor type characteristics. Further, at lower frequencies, i.e. 20 Hz, 100 Hz and 1 kHz, more dielectric dispersion is observed. The reason for higher dispersion in composite samples is the occurrence of large number of defects produced by the inequivalent displacement of dopant atoms. The phenomena of coulombic interaction inside the material causes negatively charged defects to attract positively charged defects resulting in the development of associated defect pairs. Also, the movement of oxygen vacancies in the vicinity of oxygen octahedron or back and forth motion of holes result in reorientation of dipoles. Therefore, at lower frequency, the higher dielectric constant is attributed to the contribution of (i) interfacial, (ii) electronic, (iii) dipolar and (iv) ionic polarization. At

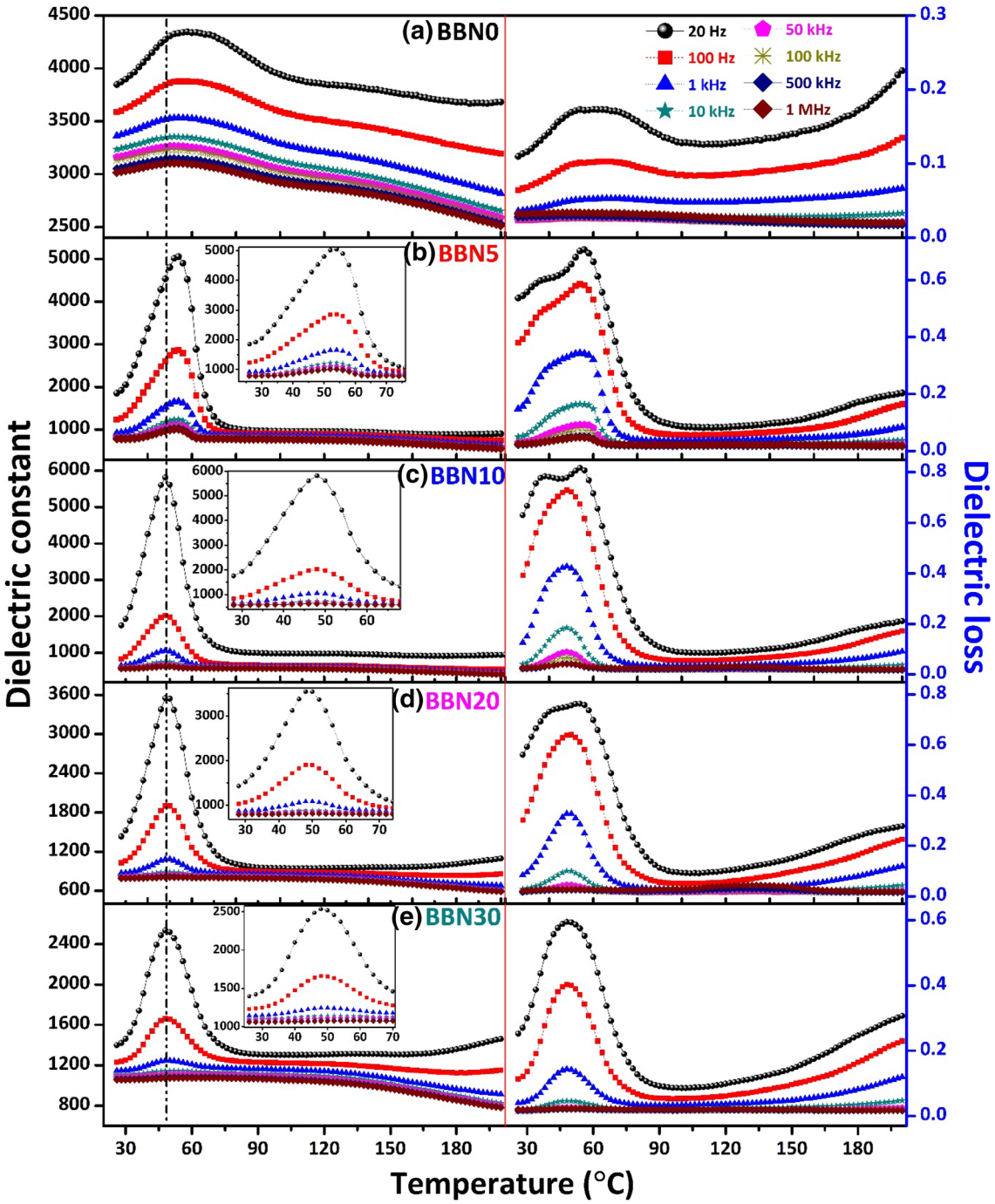

Fig. 5 Temperature dependences of dielectric constant and dielectric loss for $(1-x)$BSTZ–xBNO composites: **a** $x=0.0$, **b** $x=0.05$, **c** $x=0.10$, **d** $x=0.20$ and **e** $x=0.30$

higher frequencies, some of the polarizations do not contribute to the total polarization and only electronic and dipolar polarization are responsible for the net polarization inside the material [25]. Thus, the polarization inside the material decreases subsequently resulting in reduction in dielectric constant value at higher frequency. BBN5, BBN10 and BBN20 sample show a very good temperature stable dielectric constant at temperature higher than 75 °C. This characteristic of BSTZ–BNO composite samples can be used in high-temperature electronic switching applications. The phase transition temperature of $(1-x)$BSTZ–xBNO composites decreases gradually up to $x=0.10$. However, the Curie temperature remains nearly constant on further increasing the BCT content.

The correlation between temperature and dielectric loss is depicted in Fig. 5. Similar to dielectric constant, the dielectric loss curve also shows a dielectric loss maxima at the phase transition temperature. Above phase transition temperature, the dielectric loss decreases, becomes constant for a certain range of temperature and again increases on increasing the temperature. The dielectric loss of bare as well as composite samples is observed to be maximum at lower frequencies and decreases abruptly at higher frequencies. A gradual rise in dielectric loss of composite sample at higher temperature may be due to Debye-type relaxation of space charge at the interface between the electrodes and material, which is the typical nature of oxide-based perovskites having titanium as constituent element [26]. Moreover, ferroelectrics generally exhibit non-linear dielectric characteristics, which is due to reversible polarization in the presence of an applied electric field [27, 28]. Henceforth, their dielectric characteristics rely on both the frequency and magnitude of the applied bias voltage. In Fig. 5, it can be observed that both dielectric constant and dielectric loss were found to be dependent on the frequency of the applied ac signal. Further, at low frequency of operation, the dielectric loss curve of most of the samples is showing relaxation anomaly; this anomaly is attributed to increase in electrical conductivity at lower frequency [29]. This increase in electrical conductivity results in rapid increase and decrease in dielectric loss value around Curie temperature.

3.4 Ferroelectric studies

The Electric field versus polarization hysteresis loop of bare and composite ceramic samples at three different temperatures of 25, 75 and 125 °C is demonstrated in Fig. 6a–c. The P–E loops were recorded by applying an external electric field of up to 40 kV/cm. The inset of Fig. 6a–c show the variation of saturation polarization ($2P_s$) and remnant polarization ($2P_r$) with increasing BNO concentration. As shown in Fig. 6, all the synthesized samples exhibit ferroelectric hysteresis loops at all three temperatures. At ambient temperature, under the application of electric field, the remnant polarization and saturation polarization are found to be maximum for BBN10 specimen. Further BNO addition beyond $x = 0.10$ results in reduction of remnant and saturation polarization value. This shows that suitable BNO addition has an obvious influence in improving ferroelectric characteristics of BSTZ. The observed enhancement in the values of polarization is not intrinsic. This increased polarization demonstrated by BBN5 and BBN10 sample may be attributed to the space charge polarization effect [30] whose influence to ferroelectricity increases as BNO concentration increases in the composite. Moreover, the ferroelectric characteristics of ceramic materials are affected by their crystal phase, lattice defects like oxygen vacancies, microstructure and composition [31, 32]. Further, the structural transition occurring inside the material also controls the stability of the ferroelectric phase. It is evident that long-range polar orders of the dipoles inside the material results in superior ferroelectric properties [33]. In addition, a slight disruption in the polar ordering would affect the ferroelectricity of the material.

The observed increase in remnant polarization up to $x = 0.10$ may be due to both, reduction in leakage current and structural distortion induced by BNO addition [30, 34]. At elevated temperatures of 75 °C and 125 °C, the remnant polarization demonstrates almost identical characteristics. However, the loops were found to be slightly shifted around the origin. This abnormality can be elucidated by the existence of an internal electric field initiating from the off-centering and intrinsic movement of bound electrons inside the material. Furthermore, the area of the loop has also been increased for BBN10 sample, which may be attributed to low resistivity of the sample. The decrease in remnant polarization at higher temperatures may be ascribed to decrease in ferroelectric and increase in Para-electric phase of the materials. At room temperature, the increase in coercive field with BNO content may be attributed to dipole friction that arises owing to the domain orientation. The smaller grain size may have also contributed in enhancing the friction during domain orientation [35].

3.5 Breakdown strength measurement

Figure 7a shows the schematic diagram of breakdown measurement arrangement of a pellet. The electric breakdown strength of ceramics relies on many aspects such as grain size, porosity, etc. and extrinsic measurement constraints including electrode configuration, sample area and sample thickness [36, 37]. The external parameters for example frequency and the rate at which electric field is applied also influence the dielectric breakdown strength. Based on the above factors, it is possible that the improvement of E_{bd} in BBN10 sample is primarily due to increase in density, reduction in pore size of the material. The E_{bd} is found to be maximum for BBN10 sample, which may be ascribed to higher density among the five synthesized samples. Furthermore, as the BNO concentration rises beyond $x = 0.10$, the dielectric breakdown strength of the materials are observed to decrease. In ceramics as well as in ferroelectric composites, under an externally applied electric field, as the amount of weakly bonded ions with lower density and high porosity increases, the value of space displacement polarization also rises. Consequently, this enhancement in space displacement polarization forces the micro-pores and nano-pores inside the material to offer little resistance to electrical breakdown and deteriorate the dielectric breakdown strength [38]. Also, inner stress resulting from the non-uniform and

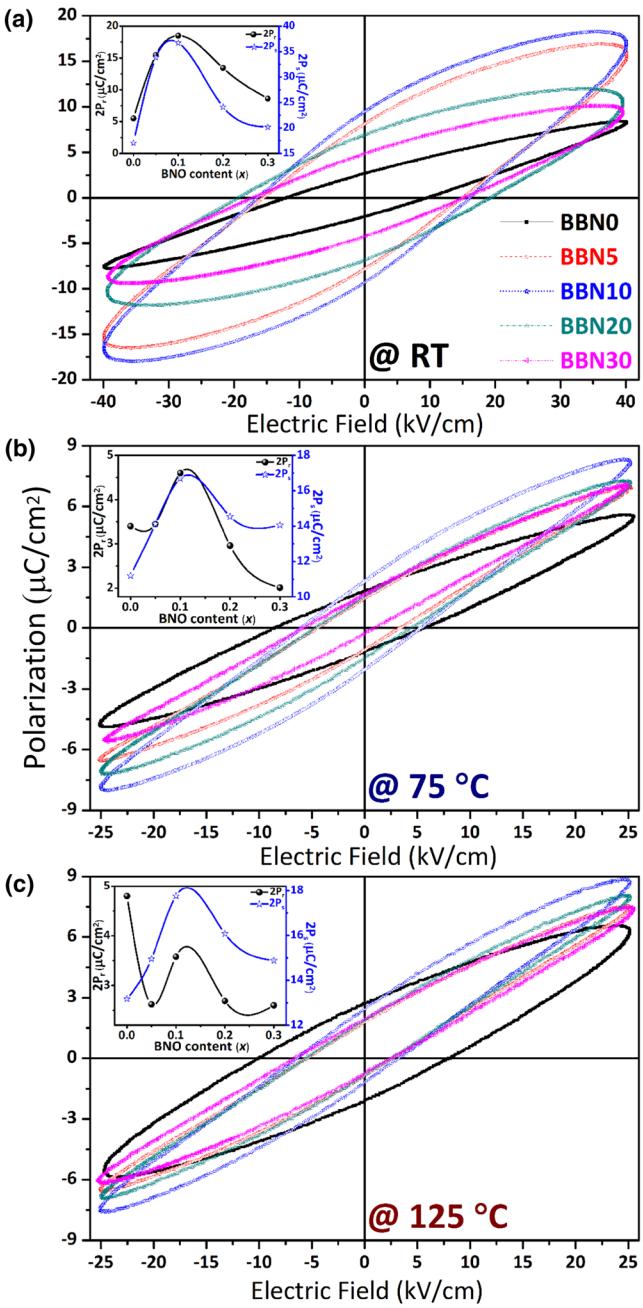

Fig. 6 Ferroelectric P–E hysteresis loops of $(1-x)$ BSTZ–xBNO at three different temperatures: **a** at room temperature, **b** at 75 °C and **c** at 125 °C; inset shows the variation in remnant polarization and saturation polarization with change in BNO content

inhomogeneous morphology can increase the ion mobility under the application of an electric field and hence reduces the E_{bd} value.

Thickness-dependent dielectric breakdown strength measurement of BBN10 specimen is depicted in the inset of Fig. 7b. As the thickness increases, there is reduction in breakdown strength. Thick dielectric pellets have the disadvantage that they possess a large number of internal and external defects such as micro-pores and micro-cracks. Figure 7c shows the schematic for breakdown of material in the presence of a micro-pore through a dendrite. Such imperfect areas are more liable to electrical breakdown, that results to a decrease in material thickness and a subsequent rise in voltage per unit thickness leading to avalanche breakdown [39]. In the present investigation, all the composites possess the same phase structure, nearly similar morphology and measurement environment. Therefore, it can be concluded that the significant enhancement in dielectric breakdown strength is mainly attributed to appropriate amount of BNO addition.

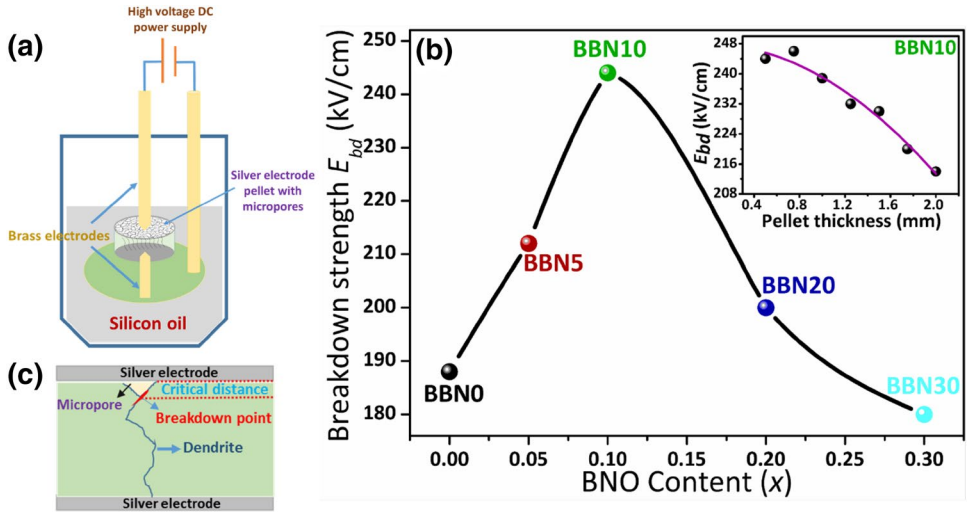

Fig. 7 **a** Schematic of dielectric breakdown strength measurement setup, **b** dielectric breakdown strength (E_{bd}) as a function of BNO content and **c** schematic showing the breakdown in any material in the presence of micropore through a dendrite

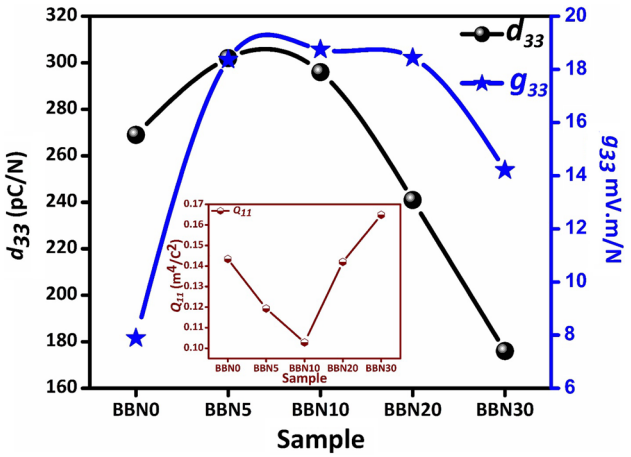

Fig. 8 Variation of piezoelectric charge coefficient (d_{33}), piezoelectric voltage constant (g_{33}) and electrostrictive constant (Q_{11}) (inset) for the $(1-x)$BSTZ–xBNO composites

3.6 Piezoelectric studies

In this study, piezoelectric response as a function of BNO content has been investigated. Figure 8 shows the variation in piezoelectric strain coefficient, piezoelectric voltage constant and electrostrictive coefficient (inset) with change in BNO content. Electrical poling conditions strongly affect the piezoelectric characteristics of any ceramic material. The domains are distributed randomly in an as-prepared material and therefore they need to be aligned in a certain direction on the application of an externally applied electric field. Typically, a high electric field is essential to attain homogeneously distributed domains, however at high electric field, the materials are prone to get damaged because of electrical breakdown. Therefore, an optimum electric field is vital to acquire superior piezoelectric properties. Moreover, poling temperature, as well as poling time, also influence the piezoelectric characteristics and therefore they are also required to be optimized. In this work, all the five cylindrical pellet specimens were poled electrically at $E \sim 18$ kV/mm for 75 min with poling temperature kept to be $T_P \sim 65$ °C, at which optimum piezoelectric characteristics were recorded. After 75 min of electrical poling, the piezoelectric charge coefficient, d_{33} did not show any significant increment and found to saturate. Further, poling a sample at an appropriate temperature results in accumulation of positive and negative charge carriers around the grain boundary interface leading to the emergence of an internal bias electric field which can increase the piezoelectric characteristics of the material. The addition of BNO results in a slight increase in piezoelectric constant for BBN5 specimen, however, it decreases with further increase in BNO concentration. It is to be worth noting that BBN10 sample still shows higher d_{33} value compared to BBN0 sample. The high value of BBN5 and BBN10 sample may be attributed to better crystallinity, high density and optimum combination of grain size and grain homogeneity in the material [19]. Another possibility for the slight increase in d_{33} value may be attributed to domain wall pinching effect with reduction in oxygen vacancy caused by BNO addition [40]. The piezoelectric voltage coefficient (g_{33}) of the five synthesized samples were measured by dividing the piezoelectric charge constant of the materials by their relative permittivity (ε). The piezoelectric constant of the material can be described by the thermodynamic theory of ferroelectricity as follows [41]:

$$d_{33} = 2\varepsilon_{33} P_r Q_{11} \quad (1)$$

where, ε_{33} represents the dielectric permittivity, P_r denotes remnant polarization and Q_{11} is the electrostrictive constant. Hence, from Eq. 1 it can be inferred that for any ceramic material with high dielectric constant and high remnant polarization may also exhibit large piezoelectric coefficient. Electrostrictive constant for the five compositions has been

evaluated using Eq. 1 and is shown in the inset of Fig. 8. An enhancement in piezoelectric properties demonstrates that BSTZ–BNO composites can prove to be a potential material for lead-free piezoelectric ceramic.

It is known that dielectric, ferroelectric and piezoelectric properties of the material are closely related to each other [42]. Further, it has also been reported that the electrical properties of the ferroelectrics are highly dependent on shape, morphology and relative density of the material [43]. Among the five synthesized materials, BBN10 has shown the optimum properties, which may solely be attributed to slightly higher relative density and comparatively homogeneous grain size of the material. So, in conclusion, the relative density of the material can be considered as the dominating mechanism among others in improving the electrical properties of the BBN10 composite. In addition, the reduction in oxygen vacancies, higher crystallinity and optimum solid solubility of BSZT and BNO may be considered as the other factors that are contributing in enhancing the electrical properties.

4 Conclusion

A new series of lead-free ceramic composite with enhanced microstructural and electrical properties were successfully synthesized. The BSTZ–BNO composites studied in this study requires lower sintering temperature for the phase formation. The co-existence of tetragonal and orthorhombic phase in the composite samples has been confirmed by Rietveld analysis. All the samples possess a polygonal grain type morphology with clearly distinguishing grain boundaries. In addition, the BSTZ–BNO composites have shown improved dielectric constant, better remnant polarization and high piezoelectric constant. These superior properties of BSTZ–BNO composites (especially BBN10) are mainly attributed to uniform grain distribution, high density of the materials and solid solubility of BNO in BSTZ up to a certain extent. At higher BNO content (BBN20 and BBN30), the dielectric constant, remnant polarization, piezoelectric constant and breakdown strength were found to decrease which indicate limited compatibility of tetragonal perovskite with orthorhombic niobate. The BSTZ–BNO composites are inexpensive and easy to fabricate. Further, the relatively homogeneous microstructure, superior electrical properties and high breakdown strength indicate that the mechano-chemical synthesis method represents a viable approach to produce such materials and can have potential application in field of ceramic capacitors.

References

1. R. Grigalaitis, M.V. Petrović, J. Bobić, A. Dzunuzovic, R. Sobiestianskas, A. Brilingas, B. Stojanović, J. Banys, Dielectric and magnetic properties of $BaTiO_3$–$NiFe_2O_4$ multiferroic composites. Ceram. Int. **40**, 6165–6170 (2014)
2. D.W. Kim, K.S. Hong, C.H. Kim, K. Char, Crystallographic orientation dependence of the dielectric constant in polymorphic $BaNb_2O_6$ thin films deposited by laser ablation. Appl. Phys. A **79**, 677–680 (2003)
3. N. Maikhuri, A.K. Panwar, A. Jha, Investigation of A-and B-site Fe substituted $BaTiO_3$ ceramics. J. Appl. Phys. **113**, 17D915 (2013)
4. J.P. Praveen, K. Kumar, A.R. James, T. Karthik, S. Asthana, D. Das, Large piezoelectric strain observed in sol–gel derived BZT–BCT ceramics. Curr. Appl. Phys. **14**, 396–402 (2014)
5. H. Zheng, F. Straub, Q. Zhan, P.L. Yang, W.K. Hsieh, F. Zavaliche, Y.H. Chu, U. Dahmen, R. Ramesh, Self-assembled growth of $BiFeO_3$–$CoFe_2O_4$ nanostructures. Adv. Mater. **18**, 2747–2752 (2006)
6. A.K. Vishwakarma, K. Jha, M. Jayasimhadri, A.S. Rao, K. Jang, B. Sivaiah, D. Haranath, Red light emitting $BaNb_2O_6$:Eu^{3+} phosphor for solid state lighting applications. J. Alloys Compd. **622**, 97–101 (2015)
7. I.-S. Cho, S.T. Bae, D.H. Kim, K.S. Hong, Effects of crystal and electronic structures of ANb_2O_6 (A=Ca, Sr, Ba) metaniobate compounds on their photocatalytic H_2 evolution from pure water. Int. J. Hydrog. Energy **35**, 12954–12960 (2010)
8. Y. Ebina, T. Higuchi, T. Hattori, T. Tsukamoto, Ferroelectric and structural properties of $Sr_{0.5}Ba_{0.5}Nb_2O_6$ thin films on $La_{0.05}Sr_{0.95}TiO_3$ substrate. Jpn. J. Appl. Phys. **45**, 7300 (2006)
9. D.W. Kim, H.B. Hong, K.S. Hong, C.K. Kim, D.J. Kim, The reversible phase transition and dielectric properties of $BaNb_2O_6$ polymorphs. Jpn. J. Appl. Phys., Part **41**, 6045–6048 (2002)
10. S.P. Gaikwad, V. Samuel, R. Pasricha, V. Ravi, Preparation of nanocrystalline ferroelectric $BaNb_2O_6$ by citrate gel method, Bull. Mater. Sci., 28 121–123 (2005)
11. M. Sahoo, Z. Yajun, J. Wang, R. Choudhary, Composition control of magnetoelectric relaxor behavior in multiferroic $BaZr_{0.4}Ti_{0.6}O_3$/$CoFe_2O_4$ composites. J. Alloys Compd. **657**, 12–20 (2016)
12. T. Takenaka, K. Maruyama, K. Sakata, $(Bi_{1/2}Na_{1/2})TiO_3$–$BaTiO_3$ system for lead-free piezoelectric ceramics. Jpn. J. Appl. Phys. **30**, 2236 (1991)
13. T. Badapanda, S. Sarangi, B. Behera, S. Parida, S. Saha, T. Sinha, R. Ranjan, P. Sahoo, Optical and dielectric study of strontium modified barium zirconium titanate ceramic prepared by high energy ball milling. J. Alloys Compd. **645**, 586–596 (2015)
14. C.C. Koch, Y. Cho, Nanocrystals by high energy ball milling. Nanostruct. Mater. **1**, 207–212 (1992)
15. L. Kong, W. Zhu, O. Tan, Preparation and characterization of $Pb(Zr_{0.52}Ti_{0.48})O_3$ ceramics from high-energy ball milling powders. Mater. Lett. **42**, 232–239 (2000)
16. Q.M. Zhang, H. Wang, N. Kim, L.E. Cross, Direct evaluation of domain-wall and intrinsic contributions to the dielectric and piezoelectric response and their temperature dependence on lead zirconate-titanate ceramics. J. Appl. Phys. **75**, 454–459 (1994)
17. G. Arlt, N.A. Pertsev, Force constant and effective mass of 90° domain walls in ferroelectric ceramics. J. Appl. Phys. **70**, 2283–2289 (1991)
18. D. Damjanovic, M. Demartin, H. Shulman, M. Testorf, N. Setter, Instabilities in the piezoelectric properties of ferroelectric ceramics. Sens. Actuators A: Phys. **53**, 353–360 (1996)
19. C.A. Randall, N. Kim, J.P. Kucera, W. Cao, T.R. Shrout, Intrinsic and extrinsic size effects in fine-grained

morphotropic-phase-boundary lead zirconate titanate ceramics. J. Am. Ceram. Soc. **81**, 677–688 (1998)
20. T.M. Kamel, G. de With, Grain size effect on the poling of soft $Pb(Zr,Ti)O_3$ ferroelectric ceramics. J. Eur. Ceram. Soc. **28**, 851–861 (2008)
21. A. Herabut, A. Safari, Processing and electromechanical properties of $(Bi_{0.5}Na_{0.5})_{(1-1.5x)}$ La_xTiO_3 ceramics. J. Am. Ceram. Soc. **80**, 2954–2958 (1997)
22. S. Sarraute, O.T. Sørensen, B.F. Sørensen, E.R. Hansen, Microstructure dependent thermophysical properties of Ni–Zn ferrite–$BaTiO_3$ functionally graded ceramics, J. Mater. Sci. **34**, 99–104 (1999)
23. A.K. Singh, T. Goel, R. Mendiratta, O. Thakur, C. Prakash, Dielectric properties of Mn-substituted Ni-Zn ferrites. J. Appl. Phys. **91**, 6626–6629 (2002)
24. A. Jain, A.K. Panwar, A.K. Jha, Influence of milling duration on microstructural, electrical, ferroelectric and piezoelectric properties of $Ba_{0.9}Sr_{0.1}Zr_{0.04}Ti_{0.96}O_3$ ceramic. Ceram. Int. **42**, 18771–18778 (2016)
25. N. Zhang, L. Li, J. Yu, High dielectric constant and good thermal stability from − 55 °C to 450 °C in $BaTiO_3$-based ceramics. Mater. Lett. **160**, 128–131 (2015)
26. X.Y. Ye, Y.M. Li, J.J. Bian, Dielectric and energy storage properties of Mn-doped $Ba_{0.3}Sr_{0.475}La_{0.12}Ce_{0.03}TiO_3$ dielectric ceramics. J. Eur. Ceram. Soc. **37**, 107–114 (2017)
27. L.H. Parker, A.F. Tasch, Ferroelectric materials for 64 Mb and 256 Mb DRAMS. IEEE Circuits Devices Mag. **6**, 17–26 (1990)
28. L. Testardi, W. Moulton, H. Mathias, H. Ng, C. Rey, Large static dielectric constant in the high-temperature phase of polycrystalline $YBa_2Cu_3O_x$. Phys. Rev. B: Condens. Matter **37**, 2324 (1988)
29. H.G. Bohn, T. Schober, Electrical conductivity of the high-temperature proton conductor $BaZr_{0.9}Y_{0.1}O_{2.95}$. J. Am. Ceram. Soc. **83**, 768–772 (2000)
30. R. Sharma, P. Pahuja, R.P. Tandon, Structural, dielectric, ferromagnetic, ferroelectric and ac conductivity studies of the $BaTiO_3$–$CoFe_{1.8}Zn_{0.2}O_4$ multiferroic particulate composites. Ceram. Int. **40**, 9027–9036 (2014)
31. S.K. Das, R.N. Mishra, B.K. Roul, Magnetic and ferroelectric properties of Ni doped $BaTiO_3$. Solid State Commun. **191**, 19–24 (2014)
32. W. Cai, C. Fu, J. Gao, H. Chen, Effects of grain size on domain structure and ferroelectric properties of barium zirconate titanate ceramics. J. Alloys Compd. **480**, 870–873 (2009)
33. M. Kuehn, H. Kliem, The method of local fields: a bridge between molecular modelling and dielectric theory. J. Electrostat. **67**, 203–208 (2009)
34. Y. Wang, C.-W. Nan, Effect of Tb doping on electric and magnetic behavior of $BiFeO_3$ thin films. J. Appl. Phys. **103**, 4103 (2008)
35. R. Muduli, R. Pattanayak, S. Raut, P. Sahu, S. V, S. Rath, P. Kumar, S. Panigrahi, R.K. Panda, Dielectric, ferroelectric and impedance spectroscopic studies in TiO_2-doped $AgNbO_3$ ceramic. J. Alloys Compd. **664**, 715–725 (2016)
36. A.L. Young, G.E. Hilmas, S.C. Zhang, R.W. Schwartz, Mechanical vs. electrical failure mechanisms in high voltage, high energy density multilayer ceramic capacitors. J. Mater. Sci. **42**, 5613–5619 (2007)
37. T. Tunkasiri, G. Rujijanagul, Dielectric strength of fine grained barium titanate ceramics. J. Mater. Sci. Lett. **15**, 1767–1769 (1996)
38. W. Lei, R. Ang, X.-C. Wang, W.-Z. Lu, Phase evolution and near-zero shrinkage in $BaAl_2Si_2O_8$ low-permittivity microwave dielectric ceramics. Mater. Res. Bull. **50**, 235–239 (2014)
39. W. Lei, Y.-Y. Yan, X.-H. Wang, W. Lu, Z.-B. Yang, W.-Z. Lu, Improving the breakdown strength of $(Mg_{0.9}Zn_{0.1})_2(Ti_{1-x}Mn_x)O_4$ ceramics with low dielectric loss. Ceram. Int. **41**, 521–525 (2015)
40. Y. Tian, S. Li, Y. Gong, D. Meng, J. Wang, Q. Jing, Effects of Er^{3+}–doping on dielectric and piezoelectric properties of $0.5Ba_{0.9}Ca_{0.1}TiO_3$–$0.5BaTi_{0.88}Zr_{0.12}O_3$–0.12%La–xEr lead–free ceramics. J. Alloys Compd. **692**, 797–804 (2017)
41. J.P. Praveen, T. Karthik, A. James, E. Chandrakala, S. Asthana, D. Das, Effect of poling process on piezoelectric properties of sol–gel derived BZT–BCT ceramics. J. Eur. Ceram. Soc. **35**, 1785–1798 (2015)
42. B. Jaffe, *Piezoelectric Ceramics*, (Elsevier, New York, 2012)
43. C. Duran, S. Trolier-McKinstry, G.L. Messing, Fabrication and electrical properties of textured $Sr_{0.53}Ba_{0.47}Nb_2O_6$ ceramics by templated grain growth. J. Am. Ceram. Soc. **83**, 2203–2213 (2000)